

Numerical and experimental analysis of thermal and flow operating conditions of waterwall tubes connected by fins

MAREK MAJDAK*
SŁAWOMIR GRĄDZIEL
WIESŁAW ZIMA
ARTUR CEBULA
MONIKA RERAK
EWA KOZAK-JAGIEŁA

Cracow University of Technology, Faculty of Environmental Engineering and Energy, Warszawska 24, 31-155 Kraków, Poland

Abstract This paper presents a method for determining the temperature distribution in the cross-section of waterwall tubes connected by fins using an in-house numerical algorithm prepared in the MATLAB environment, based on differential equations with separable variables. In order to verify the correctness of the algorithm operation, the temperature values obtained from it, determined for the frontal area of the tubes, are compared with the temperatures found in the Ansys Fluent environment and those measured on the test stand. A system corresponding to a fragment of the combustion chamber wall of a supercritical steam boiler was selected to perform the analysis. The system consists of three tubes connected by fins. The temperature distributions in the cross-sections of the tubes were compared for the case when each of the tubes was heated on one side with the same heat flux and when the heat flux falling on the central tube was by 50% higher than the heat flux incident on the neighbouring tubes. Experimental verification was carried out on a stand equipped with three vertical tubes connected by fins, heated on one side by infrared radiators.

Keywords: Heat transfer; Supercritical boiler; Waterwall tube

*Corresponding Author. Email: marek.majdak@pk.edu.pl

1 Introduction

The occurrence of thermal stresses exceeding allowable values is one of the most serious problems encountered in power boilers. In subcritical steam boilers, the temperature of the medium flowing in the tubes reaches values corresponding to the steam saturation state (Fig. 1).

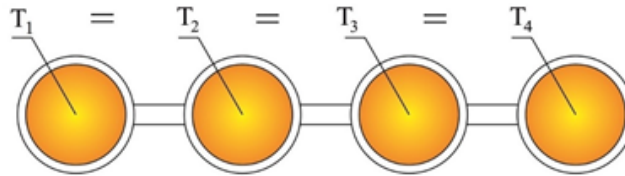


Figure 1: Temperature of the medium in waterwall tubes of subcritical steam boilers.

In supercritical steam boilers, on the other hand, the medium temperature can vary considerably in individual tubes (Fig. 2). This creates additional thermal stresses on the width of the combustion chamber wall. Therefore, it is necessary to monitor the condition of individual fragments of the waterwalls, since exceeding the allowable value of thermal stresses can lead to damage to the waterwall tubes and the fins connecting them, which necessitates the boiler repairs.

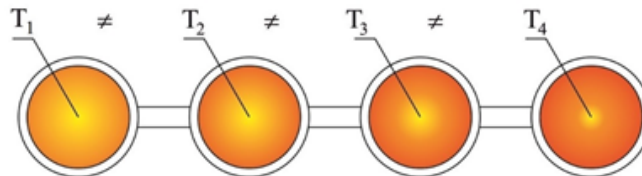


Figure 2: Temperature of the medium in waterwall tubes of supercritical steam boilers.

The literature offers numerous simplified studies taking account of averaged parameters of the medium flowing through the tubes [1], average parameters of the walls of waterwall tubes or a uniform distribution of the thermal load. Many publications analyse the issue of the heat transfer inside waterwall tubes – either by determining more precise relations that make it possible to determine the value of the heat transfer coefficient [2–4], or based on a series of experimental tests [5]. Another method of determination of temperature distribution in thick-walled element of steam pipeline based on inverse heat conduction was presented in [6]. Cases are considered where the occurrence

of the boiling crisis [7] during two-phase flows and the problems arising therefrom, with a correct description of the convective heat transfer, are taken into account; they also cover problems related to the operation of boilers at reduced thermal loads [8, 9]. Issues related to the operation of combined-cycle power plants, such as steam-gas plants, are also considered. The authors of [10] investigate the effect of individual operating parameters on the efficiency of the system, determining the conditions under which the system can achieve the highest efficiency values.

Authors of [11] presented the mathematical model for analysis of the distribution of fluid enthalpy and waterwall temperature in supercritical boiler. Proposed method is based on calculations in which were used thermophysical parameters of fluid and parameters of material of waterwall tubes computed in real-time. Moreover, many publications point to the variation in the heat flux along the combustion chamber wall width occurring in supercritical boilers. Analyses of the temperature distribution conducted for waterwalls at uniform and non-uniform heating of neighbouring tubes are presented in [12, 13]. The authors of [3, 14] discuss the heat transfer occurring in spiral waterwall tubes installed in ultra-supercritical boilers.

An analysis of the thermal conditions of a stoker boiler is presented in [15]. The authors analysed the hydrodynamic conditions occurring in the boiler combustion chamber during biomass combustion using a vibrating grate that makes it possible to change the air flow supplied from the bottom of the combustion chamber. They also investigated the effect of the distribution of the fuel mass flow and secondary air on the boiler operating parameters.

In [16], a simulation was carried out of the boiler operation under conditions of increased production of thermal energy. Cases were analysed in which the increased amount of bleed steam was directed to the heat exchanger, and the use of solutions based on an absorption heat pump, i.e. waste heat utilization, was investigated. The impact of each solution on the parameters of the boiler working medium and on the operating parameters was presented, and an economic analysis was performed of the profitability of the implementation of the solutions.

The problem of determining the technical condition of steam power plants and turbines was discussed in [17]. A method based on the Monte-Carlo simulation was proposed to analyse the results of investigations of damage to power plant components. The method takes account of the course of technological processes, their duration, as well as the failure rate and the metal remnant life. The presented model can be used to create

2.1 Initial balance equations for the medium

The mass balance equation for the control volume presented in Fig. 3 has the following form:

$$\frac{\partial(\Delta V \rho)}{\partial \tau} = (A \rho v) \Big|_{z-\frac{\Delta z}{2}} - (A \rho v) \Big|_{z+\frac{\Delta z}{2}}, \quad (1)$$

where: V – volume, m³; φ – tube inclination angle, deg; ρ – fluid density, m³/kg; τ – time, s; A – surface area, m²; v – fluid velocity, m/s; Δz – analysed control volume length in the fluid flow direction, m.

Considering a constant cross-section of the analysed tube and assuming that the fluid density in the entire volume is equal to the fluid density at the control volume centre, and assuming further that the control volume is infinitely small, Eq. (1) can be expressed as

$$\frac{\partial \rho}{\partial \tau} = - \frac{\partial(\rho v)}{\partial z}, \quad (2)$$

or

$$\frac{\partial \rho}{\partial \tau} = - \frac{1}{A} \frac{\partial \dot{m}}{\partial z}, \quad (3)$$

where: \dot{m} – fluid mass flow rate, kg/s.

The fluid mass flow rate is defined by the following relation:

$$\dot{m} = A v \rho. \quad (4)$$

The next balance equation is the momentum conservation equation, which has to take account of the rate of changes in the momentum accumulated in the control volume, the momentum fluxes flowing into and out of the control volume, and all the forces acting on the control volume. The following forces have to be taken into consideration: the forces exerted by the fluid on the tube wall, the forces opposite to vectors normal to the inlet and the outlet cross-section of the analysed control volume and the friction force between the fluid and the tube wall. The momentum conservation equation for the control volume under analysis can be written as

$$\begin{aligned} \frac{\partial}{\partial \tau} (A v \rho \Delta z) &= (\dot{m} v) \Big|_{z-\frac{\Delta z}{2}} - (\dot{m} v) \Big|_{z+\frac{\Delta z}{2}} + A \left(p \Big|_{z-\frac{\Delta z}{2}} - p \Big|_{z+\frac{\Delta z}{2}} \right) \\ &\quad - \sigma_{\tau} U \Delta z - \rho g \Delta V \sin \varphi, \end{aligned} \quad (5)$$

where: g – gravitational acceleration, m/s²; p – pressure, Pa; U – tube perimeter, m; σ_{τ} – tangential stresses, N/m².

Considering that the control volume length is infinitely small and determining the pressure related to the friction force and the fluid velocity, Eq. (5) can be rearranged to

$$\frac{\partial \dot{m}}{\partial \tau} = -\frac{1}{A} \frac{\partial}{\partial z} \left(\frac{\dot{m}^2}{\rho} \right) - A \left(\frac{\partial p}{\partial z} + \frac{\partial p_\tau}{\partial z} + \rho g \sin \varphi \right), \quad (6)$$

where: p_τ – pressure related to the friction force, Pa.

The internal energy balance of the fluid, related to a unit of its mass, must take account of kinetic energy, both potential and internal. It can be expressed using formula

$$e = \frac{v^2}{2} + gz \sin \varphi + u, \quad (7)$$

where: e – energy per mass, J/kg; u – unit internal energy, J/kg.

In order to simplify the formula for the purposes of the case under analysis, it is assumed that the work done by volume and surface forces is negligibly small. The relations describing individual forms of energy are presented in detail in [22]. After appropriate simplifications and rearrangements, Eq. (7) can be written in the form of a differential equation with separable variables, i.e.:

$$\frac{\partial i}{\partial \tau} = \left(1 - \frac{1}{\rho} \frac{\partial p}{\partial i} \right)^{-1} \left[\frac{\dot{m}}{A\rho} \left(\frac{1}{\rho} \frac{\partial p}{\partial z} - \frac{\partial i}{\partial z} + \frac{1}{\rho} \frac{\partial p_\tau}{\partial z} \right) + \frac{4h(\theta - t)}{d_{\text{in}}\rho} - \frac{1}{A\rho} \frac{\partial p}{\partial \rho} \frac{\partial \dot{m}}{\partial z} \right], \quad (8)$$

where: d_{in} – tube inner diameter, m; i – enthalpy, J/kg; t – fluid temperature, °C; h – heat transfer coefficient, W/(m²·K); θ – tube wall temperature, °C.

2.2 Solving balance equations for the fluid

Properly modified, the relations expressed in Eqs. (1)–(8) will enable determination of the distributions of the fluid mass flow rate, pressure and enthalpy. Reduced to the form of differential equations with separable variables, they will become the basis for a mathematical model enabling the analysis of the thermal and flow phenomena occurring in the boiler water-wall tubes. In their final version, the balance equations are written in a form

with time derivatives on one side of the equation and space derivatives on the other [23].

The derivatives are then replaced with difference quotients:

- energy balance equation:

$$\frac{\partial i}{\partial z} = \frac{A\rho}{\dot{m}} \left[-\frac{\partial i}{\partial \tau} + \frac{4h(\theta - t)}{d_{in}\rho} \right], \quad (9)$$

applying the method of lines, the following is obtained:

$$\frac{di_j^\tau}{dz} = \frac{A\rho_j^{\tau-\Delta\tau}}{\dot{m}_j^{\tau-\Delta\tau}} \left[-\frac{h_j^\tau - h_j^{\tau-\Delta\tau}}{\Delta\tau} + \frac{4h_j^{\tau-\Delta\tau} (\theta_j^{\tau-\Delta\tau} - t_j^{\tau-\Delta\tau})}{d_{in}\rho_j^{\tau-\Delta\tau}} \right], \quad (10)$$

- mass balance equation:

$$\frac{\partial \dot{m}}{\partial z} = -A \frac{\partial \rho}{\partial \tau}, \quad (11)$$

applying the method of lines, the equation is expressed as

$$\frac{d\dot{m}_j^\tau}{dz} = -A \frac{\rho_j^\tau - \rho_j^{\tau-\Delta\tau}}{\Delta\tau}, \quad (12)$$

- momentum balance equation:

$$\frac{\partial}{\partial z} \left(\frac{\dot{m}^2}{A^2\rho} + p \right) = -\frac{1}{A} \frac{\partial \dot{m}}{\partial \tau} - \frac{\partial p_\tau}{\partial z} - \rho g \sin \varphi, \quad (13)$$

applying the method of lines, the equation is expressed as

$$\frac{d}{dz} \left[\frac{(\dot{m}^2)_j^\tau}{A^2\rho_j^\tau} + p_j^\tau \right] = -\frac{1}{A} \frac{(\dot{m}^2)_j^\tau - (\dot{m}^2)_j^{\tau-\Delta\tau}}{\Delta\tau} - \frac{dp_\tau}{dz} - \rho_j^\tau g \sin \varphi. \quad (14)$$

The relations prepared in this way were used in the numerical program to determine the temperature distribution of the fluid flowing through the waterwall tubes. The numerical model assumes that the water temperature will be the same throughout the entire cross-section of the tube. It is determined in each cross-section at each time step on the basis of differential equations describing the principles of conservation of mass, momentum and energy.

2.3 Energy balance equations for waterwall tube walls

The time- and space-dependent distribution of the temperature of waterwall tubes was determined using the transient heat conduction equation. For the purposes of the model, it is assumed that the entire pitch of spacing of a single tube in the cross-section under analysis is heated with an identical heat flux. The numerical model ensures determination of thermodynamic parameters at each of the set characteristic points of the walls of the tubes and of the fins connecting them, in each time step, which makes it possible to achieve high accuracy of the results. The temperature distribution inside the walls of the waterwall tubes was established using the division proposed in [24, 25] and presented in Fig. 4.

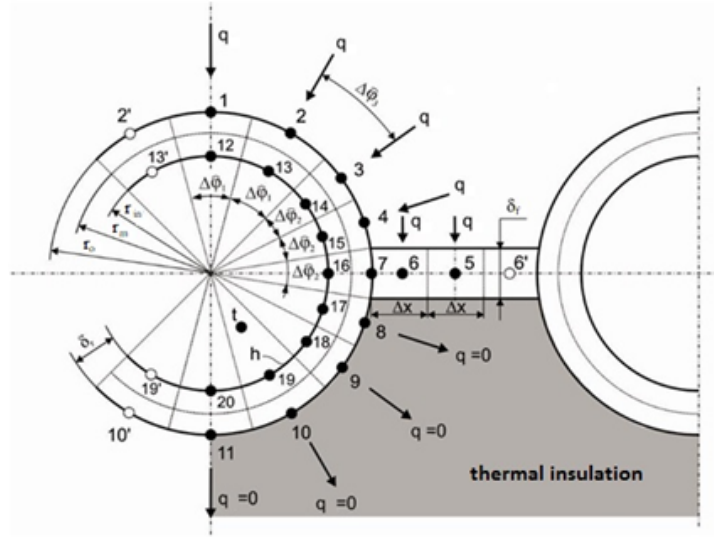


Figure 4: Division of the cross-section of a tube with a fin into control volumes.

The cross-section of the tube-fin connection was divided into control volumes (Fig. 4). Energy balance equations were written for each node. An example equation, for Point 1, is presented below:

$$\begin{aligned}
 c_1 \rho_{1,j} \frac{\Delta \hat{\varphi}_1}{2} (r_o^2 - r_m^2) \Delta z \frac{d\theta_{1,j}}{d\tau} &= k_{1,j} \frac{\theta_{2,j} - \theta_{1,j}}{\Delta \hat{\varphi}_1 r_o} \delta_t \Delta z \\
 &+ k_{1,j} \frac{\theta_{12,j} - \theta_{1,j}}{\delta_t} \Delta \hat{\varphi}_1 r_m \Delta z + k_{1,j} \frac{\Delta \hat{\varphi}_1}{2} (r_o^2 - r_m^2) \frac{\theta_{1,j-1} - \theta_{1,j}}{\Delta z} \\
 &+ k_{1,j} \frac{\Delta \hat{\varphi}_1}{2} (r_o^2 - r_m^2) \frac{\theta_{1,j+1} - \theta_{1,j}}{\Delta z} + q_j \Delta \hat{\varphi}_1 r_o \Delta z, \quad (15)
 \end{aligned}$$

where: c – specific heat, J/(kg·K); δ_t – tube wall thickness, m; Δz – assumed length of the tube section, m; r_m – mean radius of the tube, m; r_o – tube outer radius, m; k – heat conductivity coefficient, W/(m·K).

After rearrangements, a relation is obtained that makes it possible to determine temperature at Point 1 (see Fig. 4):

$$\begin{aligned} \theta_{1,j}^{\tau+\Delta\tau} = \theta_{1,j}^{\tau} + \frac{\Delta\tau}{c_{1,j}^{\tau}\rho_{1,j}^{\tau}\frac{\Delta\hat{\varphi}_1}{2}(r_o^2 - r_m^2)\Delta z} & \left[k_{1,j}^{\tau} \frac{\theta_{2,j}^{\tau} - \theta_{1,j}^{\tau}}{\Delta\hat{\varphi}_1 r_o} \delta_t \Delta z \right. \\ & + k_{1,j}^{\tau} \frac{\theta_{12,j}^{\tau} - \theta_{1,j}^{\tau}}{\delta_t} \Delta\hat{\varphi}_1 r_m \Delta z + k_{1,j}^{\tau} \frac{\Delta\hat{\varphi}_1}{2} (r_o^2 - r_m^2) \frac{\theta_{1,j-1}^{\tau} - \theta_{1,j}^{\tau}}{\Delta z} \\ & \left. + k_{1,j}^{\tau} \frac{\Delta\hat{\varphi}_1}{2} (r_o^2 - r_m^2) \frac{\theta_{1,j+1}^{\tau} - \theta_{1,j}^{\tau}}{\Delta z} + q_j^{\tau} \Delta\hat{\varphi}_1 r_o \Delta z \right]. \quad (16) \end{aligned}$$

Writing down the equations, developed in the same manner as for Eqs. (15)–(16), for all 20 elements, makes it possible to create a matrix of coefficients describing the temperature distribution in a half of the cross-section of a single waterwall tube connected to a fin. Further expansion of the model, for a system of several connected tubes, is carried out in the same way.

3 Numerical verification of the proposed method

In order to verify the correctness of the results obtained from the numerical algorithm, calculations and a comparative simulation were carried out based on the operating parameters of an 858 MW supercritical power boiler installed in a power plant in Poland. A system consisting of three tubes connected by fins was adopted for the analysis. Water with mass flow of an 0.77 kg/s and pressure 29.96 MPa flows into each tube with outer diameter 33.7 mm and wall thickness 6.1 mm. The length of the tube element is assumed to be 0.5 m and the time step is determined in each iteration using the Courant-Friedrichs-Lewy condition. The system characteristic points were determined as presented in Fig. 5.

The results are presented using the temperature distributions obtained 45 m from the inlet. Two cases were analysed: the heat flux falling on the tubes has an identical value (case 1) and the central tube is heated with a heat flux by 50% higher compared to the heat flux incident on the pitches of spacing of the neighbouring tubes (case 2). The temperature values obtained from the numerical model and the values from the simulation carried

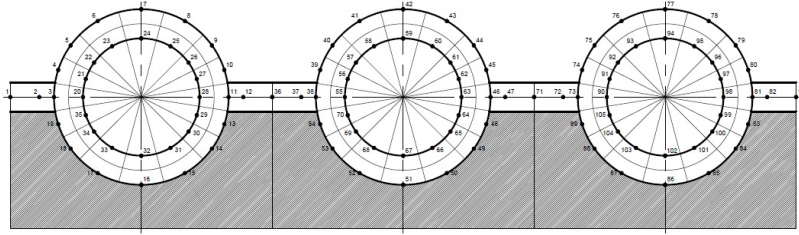


Figure 5: Division of the cross-section of three tubes with fins into control volumes.

out in the Ansys Fluent environment are presented. In Ansys Fluent analysed system was divided to 15 m parts due to problems with calculations. There was used the quadrilateral mesh with a size of $1\text{ mm} \times 1\text{ mm}$ for the cross-sections of the analysed model and with an element length of 5 cm in the direction of the tube length. In order to define the correctness of the results obtained from the numerical model and the CFD model, the relative error was calculated from the following relation:

$$e_{CFD} = \frac{|\theta_{CFD} - \theta_{MOD}|}{\theta_{CFD}} \times 100\%, \quad (17)$$

where: e_{CFD} – relative error in the wall temperature determination, %; θ_{MOD} – wall temperature determined using the numerical algorithm, K; θ_{CFD} – wall temperature obtained from the Ansys Fluent program, K.

Figures 6 and 7 illustrate the analysis for uniformly heated tubes. Figure 6 presents the temperature distribution in the tubes and fins found using the proposed algorithm, whereas Fig. 7 shows the temperature distribution produced by the CFD model. Table 1 presents a comparison between the results produced by the proposed model and the CFD simulation. It also shows the calculated relative error.

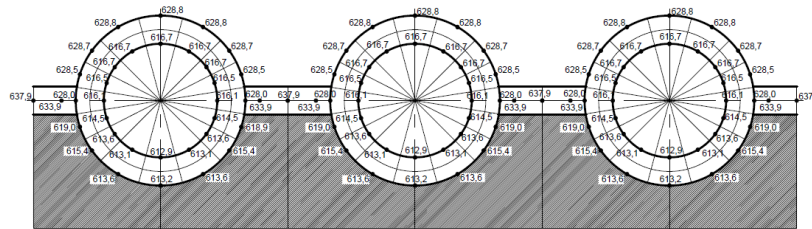


Figure 6: Temperature values (given in Kelvin scale) obtained in selected characteristic points at uniform heating of the system.

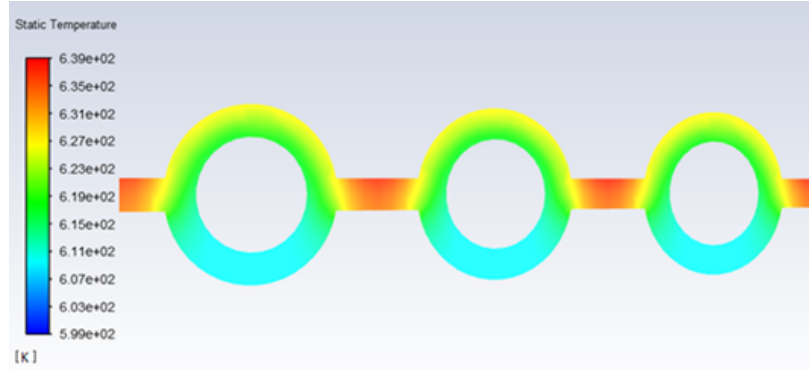


Figure 7: Temperature distribution (given in Kelvin scale) obtained from the CFD model at uniform heating of the tubes.

Table 1: Comparison of temperature values at selected points – uniform heating of the system.

Characteristic point number	Temperature from the CFD model, θ_{CFD} , K	Temperature from the numerical model, θ_{MOD} , K	Temperature difference, K	Relative error e_{CFD} , %
7	627.7	628.8	1.1	0.18
16	611.8	613.2	1.4	0.22
42	627.7	628.8	1.1	0.18
51	611.8	613.2	1.4	0.22
77	627.7	628.8	1.1	0.18
86	611.8	613.2	1.4	0.22

Figures 8 and 9 illustrate the analysis for non-uniformly heated tubes. Figure 8 presents the temperature distribution in the tubes and fins found using the proposed algorithm, whereas Fig. 9 shows the temperature distribution produced by the CFD model at non-uniform heating of the tubes. Table 2 presents a comparison between the results produced by the proposed model and the CFD simulation. It also shows the calculated relative error.

Analysing Figs. 6–9 and Tables 1–2, it can be seen that the obtained temperature distributions demonstrate high convergence. The differences between the results obtained from the numerical model and the simulation are quite small. The maximum relative error in the presented comparisons is $e_{\text{CFDmax}} = 0.31\%$. The largest discrepancies in the temperature distribution

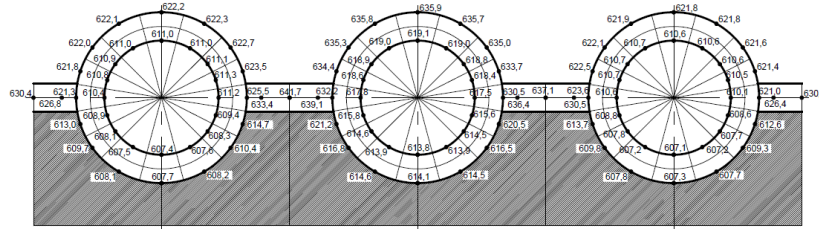


Figure 8: Temperature values (given in Kelvin scale) obtained in selected characteristic points at non-uniform heating of the system.

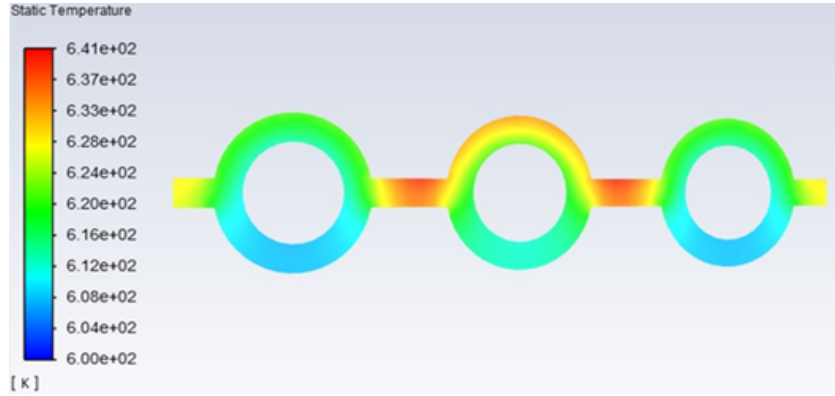


Figure 9: Temperature distribution (given in Kelvin scale) obtained in the Ansys Fluent environment at non-uniform heating of the system.

Table 2: Comparison of temperature values at selected points – non-uniform heating of the system.

Characteristic point number	Temperature from the CFD model, θ_{CFD} , K	Temperature from the numerical model, θ_{MOD} , K	Temperature difference, K	Relative error e_{CFD} , %
7	622.9	622.2	0.7	0.11
16	609.4	607.7	1.7	0.28
42	634.3	635.9	1.6	0.25
51	614.3	614.1	0.2	0.03
77	621.8	621.8	0.0	0.00
86	609.3	607.3	1.9	0.31

can be seen at the centre of the fins connecting the tubes. They are due to the way, adopted in the numerical model, of dividing the cross-section of the analysed tubes into control volumes.

The results presented above indicate that the proposed algorithm can successfully be applied to determine the temperature distribution in several adjacent waterwall tubes heated uniformly. The simulation results can be used as input data while determining the stress distribution in the analysed model section.

4 Experimental verification of the proposed method

In order to confirm the correctness of the results obtained using the numerical model, a test stand was designed and built. A detailed description of the stand structure can be found in [26].

The main elements of the stand are three tubes connected to each other by fins imitating a fragment of the combustion chamber wall. The tubes and the fins are made of P265GH steel with known thermophysical properties. According to the assumptions made earlier, the tubes were thermally insulated on one side and connected to a cooling water tank. Systems of heat radiators connected to power controllers were installed in front of the tubes, which made it possible to simulate the operation of a system heated on one side non-uniformly or uniformly. Figure 10 shows a diagram of the test stand, along with the location of the thermocouples installed in specific measuring sections. A Wilo Stratos GIGA 40/1-45/3,8 pump was used to ensure a stabilized flow of water; the pump main parameters are listed in Table 3 [27].

Table 3: Circulation pump technical data.

Parameter and unit	Value
Elevation head, m	1–45
Power supply, V	3×400
Pump motor power, kW	3.8
Allowable range of rotational speed, rpm	500–4000
Pumped fluid temperature, °C	–20 + 140
Maximum working pressure, bar	16

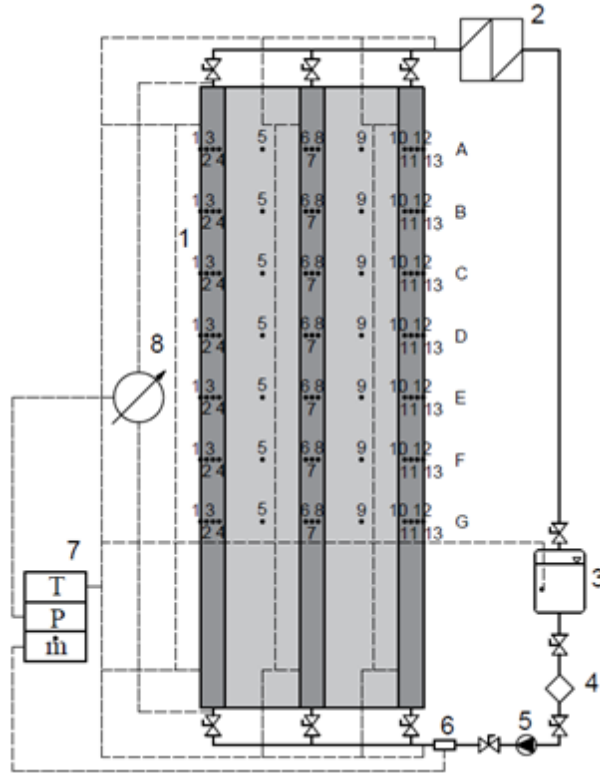


Figure 10: Diagram of the test stand: 1 – system of tubes connected by fins, 2 – cooler, 3 – circulating water tank, 4 – contamination filter, 5 – circulation pump, 6 – flowmeter, 7 – data acquisition system, 8 – power control system for the heating elements.

The pump installed on the test stand makes it possible to pump high-temperature water over a wide range of output and rotational speed. The operating parameters can be changed using an inverter. The pump circulates water through the test stand and the system of tubes connecting it to the tank. Due to that, the rise in the temperature of the medium flowing in the circulation loop occurs quite quickly.

In order to ensure one-side uniform heating of the tubes installed on the test stand, a system of radiant heaters was applied. The radiant heaters were connected in rows on a frame placed parallel to the tubes along the length of the selected test section. In each of the three rows, eight 1000W Victory/Philips HeLeN radiant heaters were installed. The radiant heaters were mounted in IRZ1000 housings, making it possible to properly direct

the radiation beams. The deviation of the side walls of the housings was wide enough to enable heating of the fins connecting the tubes with a heat flux similar to that incident on the tubes. The radiant heaters were placed on a supporting structure locating them at a distance of about 10 cm from the heated elements. According to the manufacturer's data, this location makes it possible to obtain the highest heat flux value. By connecting each of the radiant systems to a power controller, it was possible to set the value of the heat flux falling on each pitch of spacing of the waterwall tubes according to current needs. Three BTE-435 power controllers were used to regulate the power of the rows of the infrared radiators. Their basic parameters are listed in Table 4 [28].

Table 4: Parameters of the BTE-435 power controller module.

Parameter and unit	Value
Operating range, kW	0–10
Accuracy, % of power	1.0
AC voltage, V	230
Maximum output current, A	80

The water flow in the system was measured using an MPP 600 flowmeter made by ENKO-POMIAR Sp. z o.o. The main advantages of the flowmeter include the lack of moving parts and a flow diameter close to the diameter of the pipe supplying water to the vertical tubes. Owing to that, no additional losses arise in the system. The flowmeter most important parameters are presented in Table 5 [29].

Table 5: Parameters of the ENKO-POMIAR Sp. o.o. MPP 600 flowmeter.

Parameter	Value
Measuring range, m/s	0–10
Accuracy, % of the flow rate	0.2–1.0
Allowable working medium	Water; current-carrying, inert or chemically aggressive liquids
Current output signal, mA	4–20

NiCr-NiAl jacket thermocouples manufactured by ALF-SENSOR Sp. j. [30] were used to measure the temperature of water flowing into the measuring section and for selected points on the face of the tubes and the connecting fins. The thermocouples were attached to the stand using thermal paste and

neodymium magnets with increased resistance to high temperatures. The permissible temperature range for this type of sensors is -40°C – 1000°C , the permissible deviation of sensor readings in the range of -40°C – 375°C is $\pm 1.5^{\circ}\text{C}$, in the range of 375°C – 1000°C the permissible deviation is ± 0.004 of the temperature value expressed in degrees Celsius.

The data indicated by the described measuring devices were recorded using an Ahlborn ALMEMO MA 5690-2 data acquisition system [31]. The acquisition system cooperates with the AMR Win Control software [32], intended for analysing data from Ahlborn devices and enabling the export of results to a spreadsheet.

Numerical calculations and measurements were made for cases in which the tubes were heated uniformly and for cases in which the heat flux falling on the central tube was different compared to the outermost tubes. In each measuring series, at each tube inlet, water reached the pressure of $p = 1.4 \text{ MPa}$ and the temperature of $t = 313 \text{ K}$, and the average mass flow rate of water was $\dot{m} = 0.278 \text{ kg/s}$. The following data were adopted in the numerical model: spatial step $\Delta z = 5 \text{ cm}$, time step $\tau = 0.1 \text{ s}$. Eight radiators were installed along each tube (24 in total). The surface area of irradiation with eight radiators is $A = 0.84 \text{ m}^2$. The highest achievable heat flux is $q = 9500 \text{ W/m}^2$. The test stand at the time of the measurements is shown in Fig. 11.

In order to define the correctness of the results obtained from the numerical model and of the measuring data, the relative error was calculated from the following formula:

$$e_{\text{MES}} = \frac{|\theta_{\text{MES}} - \theta_{\text{MOD}}|}{\theta_{\text{MES}}} \times 100\%, \quad (18)$$

where: e_{MES} – relative error in the wall temperature determination, %; θ_{MOD} – temperature determined using the numerical algorithm, K; θ_{MES} – temperature measured on the test stand, K.

Table 6 presents the results for selected points located on the outer frontal surface of individual tubes (marked in the system diagram (Fig. 10) as 3 (it corresponds Point 7 in Fig. 5), 7 (it corresponds Point 42 in Fig. 5) and 11 (it corresponds Point 77 in Fig. 5)). The tubes were heated using radiators operating at 80% of their maximum power. The mean heat flux falling on the pitch of spacing of the waterwall tubes is $q = 7.600 \text{ W/m}^2$. Considering that, according to the characteristics of the applied radiators, the heat flux reaching the analysed fragment is strongly dependent on the distance from the radiator, the results obtained for the points closest to



Figure 11: Tests stand at the time of the measurements.

the radiators are burdened with the smallest errors. The maximum relative error in the presented comparisons totals $e_{\text{MESmax}} = 0.71\%$.

Table 7 presents the results for selected points located at the centres of individual tubes in the case of non-uniform heating. It presents the results for the same points as in the case of uniform heating of the tubes (Points: 3, 7, and 11). The central tube was heated using radiators operating at 80% of maximum power. The heat flux falling on the pitch of spacing of the central tube is $q = 7.600 \text{ W/m}^2$. The outermost tubes were heated using radiators operating at 60% of their maximum power. The heat flux falling on the pitch of their spacing was $q = 5.700 \text{ W/m}^2$. The maximum relative error in the presented comparisons totals $e_{\text{MESmax}} = 1.0\%$.

To summarize, it can be noted that there are differences in tube temperature values obtained using the numerical algorithm and measured on the test stand methods do not exceed 2.5 K for uniform heating of the analysed system (maximum relative error is 0.71%) and do not exceed 3.5 K for non-

Table 6: Temperature distribution obtained at uniform heating of the analysed system for different measuring levels.

Measuring point	Measured temperature θ_{MES} , K	Calculated temperature θ_{MOD} , K	Temperature difference, K	Relative error e_{MES} , %
B3	324.5	324.9	0.4	0.12
B7	324.7	324.9	0.2	0.06
B11	324.1	324.9	0.8	0.25
D3	324.3	323.2	1.1	0.34
D7	325.5	323.2	2.3	0.71
D11	324.1	323.2	0.9	0.28
F3	318.5	318.4	0.1	0.03
F7	320.1	318.4	1.7	0.53
F11	317.3	318.4	1.1	0.35

Table 7: Temperature distribution obtained at non-uniform heating of the analysed system for different measuring levels.

Measuring point	Measured temperature θ_{MES} , K	Calculated temperature θ_{MOD} , K	Temperature difference, K	Relative error e_{MES} , %
B3	320.9	323.6	2.7	0.84
B7	322.0	325.0	3.0	0.93
B11	320.4	323.6	3.2	1.00
D3	320.0	321.4	1.4	0.44
D7	320.3	323.0	2.7	0.84
D11	319.7	321.4	1.7	0.53
F3	316.4	317.2	0.8	0.25
F7	318.7	318.3	0.4	0.13
F11	316.6	317.2	0.6	0.19

uniform heating of the analysed system (maximum relative error is 1.00%). One of the main reasons for the occurrence of temperature differences between the results obtained from the numerical model and the measurements were the problems related to the correct attachment of thermocouples to the surface of the system under consideration. Analysing the errors for the obtained experimental results and those produced by the numerical calcu-

lations, it can be concluded that the proposed numerical algorithm provides satisfactory computing accuracy. Owing to that, the results obtained from it can be used, for example, to determine the stress distribution for the analysed area.

5 Conclusions

The paper presents a numerical model for the analysis of thermal and flow phenomena occurring in smooth tubes connected by fins. The model basic assumptions are presented, along with the way in which the cross-section of the analysed system is divided into control volumes. Unlike the solutions presented in most to-date studies, the proposed model makes it possible to determine the temperature distribution in a few waterwall tubes connected by fins. This in turn enables correct simulation of the operation of the combustion chamber walls of sub- and supercritical boilers. By determining the parameters of the fluid and the tube walls in each time step, and using a variable time step, the accuracy of the results was improved. The temperature distribution determined for selected characteristic points, after approximation for the remaining part of the cross-section, can be used to establish the distribution of thermal stresses, for example to identify fragments with the highest hazard of the occurrence of stresses exceeding allowable values.

The numerical algorithm results were verified by comparison with the temperature distribution obtained from CFD calculations. The temperature for points on the centre of front wall of analysed tubes obtained from CFD model is 627.7 K and 628.8 K for results from the numerical model – for the case in which tubes are heated with the same heat flux. For the non-uniform heated tubes the temperature for point on the centre of front wall of centre tube obtained from CFD model is 634.3 K and 635.9 K for results from the numerical model, and for the side tubes accordingly 622.9 K/621.8 K for results from CFD calculations and 622.2 K/621.8 K for numerical algorithm results.

The numerical algorithm results were also verified by comparison with the measurements on the prepared test stand. Considering that the stand had to simulate possibly uniform heating of the entire pitch of spacing of the tubes connected by the fins, a system was used of infrared radiators placed in parallel to three heated tubes. Comparing the simulation results and the experimentally measured temperatures with the results produced

by the numerical algorithm, high convergence was found between them. The highest temperatures for points on the centre of front wall of analysed tubes obtained from measurements are within the range 324.1–324.7 K and the highest temperature for results from the numerical model is equal to 324.9 K – for the case in which tubes are heated with uniform heat flux. For the non-uniform heated tubes the highest temperature for point on the centre of front wall of centre tube obtained from measurements is 322.0 K and 325.0 K for results from the numerical model, and for the side tubes accordingly 320.9 K/320.4 K for results from measurements and 323.6 K/323.6 K for numerical algorithm results.

It is therefore concluded that the proposed numerical model enables correct determination of the temperature distribution in the waterwall tubes and in the fins connecting them, both at uniform and non-uniform heating of individual pitches of spacing of the tubes making up the analysed system. The solutions applied on the test stand enabled satisfactory simulation of the conditions occurring in the combustion chamber. The determined temperature distribution can be used to establish the distribution of thermal stresses for the cross-section of the analysed model.

Acknowledgements

The research leading to the presented results was financed from the 2014–2021 Norwegian Funds through the National Centre for Research and Development (Grant NOR/POLNORCCS/0015/2019-00).

Received 24 October 2023

References

- [1] Jackson J.D.: *Fluid flow and convective heat transfer to fluids at supercritical pressure*. Nucl. Eng. Des. **264**(2013), 24–40.
- [2] Taler D.: *A new heat transfer correlation for transition and turbulent fluid flow in tubes*. Int. J. Therm. Sci. **108**(2016), 108–122.
- [3] Grądziel S., Majewski K., Majdak M., Mika Ł., Sztekler K., Kobylecki R., Zarzycki R., Pilawska M.: *Testing of heat transfer coefficients and frictional losses in internally ribbed tubes and verification of results through CFD modelling*. Energies **15**(2022), 207.
- [4] Granda M., Trojan M., Taler D.: *CFD analysis of steam superheater operation in steady and transient state*. Energy **199**(2020), 117423.

-
- [5] Węglowski B.: *Identification of Thermal Operating Conditions of Boiler Furnace Tube*. Zeszyty Naukowe Politechniki Krakowskiej **2**(1995). Wydaw. PK, Kraków 1995 (in Polish).
- [6] Grądziel S.: *Determination of temperature and thermal stresses distribution in power boiler elements with use inverse heat conduction method*. Arch. Thermodyn. **32**(2011), 3, 191–200.
- [7] Huang C.N., Kharangate C.R.: *A new mechanistic model for predicting flow boiling critical heat flux based on hydrodynamic instabilities*. Int. J. Heat Mass Tran. **138**(2019), 1295–1309.
- [8] Zima W., Taler J., Grądziel S., Trojan M., Cebula A., Ocloń P., Dzierwa P., Taler D., Rerak M., Majdak M., Korzeń A., Skrzyniowska D.: *Thermal calculations of a natural circulation power boiler operating under a wide range of loads*. Energy **261**(2022), 125357.
- [9] Taler J., Trojan M., Dzierwa P., Kaczmarek K., Węglowski B., Taler D., Zima W., Grądziel S., Ocloń P., Sobota T., Rerak M., Jaremkiwicz M.: *The flexible boiler operation in a wide range of load changes with considering the strength and environmental restrictions*. Energy **263**(2023), 125745.
- [10] Khan M.: *Performance of a combined cycle power plant due to auxiliary heating from the combustion chamber of the gas turbine topping cycle*. Arch. Thermodyn. **42**(2021), 1, 147–162.
- [11] Zima W., Grądziel S., Cebula A.: *Modelling of heat and flow phenomena occurring in waterwall tubes of boilers for supercritical steam parameters*. Arch. Thermodyn. **31**(2010), 3, 19–36.
- [12] Qu M., Yang D., Liang Z., Wan L., Liu D.: *Experimental and numerical investigation on heat transfer of ultra-supercritical water in vertical upward tube under uniform and non-uniform heating*. Int. J. Heat Mass Tran. **127**(2018), 769–783.
- [13] Kong X., Li H., Zhang Q., Guo K., Luo Q., Lei X.: *A new criterion for the onset of heat transfer deterioration to supercritical water in vertically-upward smooth tubes*. Appl. Therm. Eng. **151**(2019), 66–76.
- [14] Wang S., Yang D., Zhao Y., Qu M.: *Heat transfer characteristics of spiral water wall tube in a 1000 MW ultra-supercritical boiler with wide operating load mode*. Appl. Therm. Eng. **130**(2018), 501–514.
- [15] Kobylecki R., Zarzycki R., Bis Z., Panowski M., Wiłski M.: *Numerical analysis of the combustion of straw and wood in a stoker boiler with vibrating grate*. Energy **222**(2021), 119948.
- [16] Panowski M., Zarzycki R., Kobylecki R.: *Conversion of steam power plant into cogeneration unit – case study*. Energy **231**(2021), 120872.
- [17] Sultanov M.M., Griga S.A., Ivanitckii M.S., Konstantinov A.A.: *Monte-Carlo method for assessing and predicting the reliability of thermal power plant equipment*. Arch. Thermodyn. **42**(2021), 4, 87–102.
- [18] MATLAB R2019b Update 5 (9.7.0 1319299). The MathWorks Inc. 2020.
- [19] Ansys Workbench 2019 R3 19. 5.0. 2019072818. ANSYS Inc. 2019.

- [20] Majdak M., Grądziel S.: *Influence of thermal and flow conditions on the thermal stresses distribution in the evaporator tubes*. Energy **209**(2020), 118416.
- [21] Zima W., Grądziel S.: *Simulation of transient processes in heating surfaces of power boilers: Mathematical modelling and experimental verification*. LAP Lambert Academic Publishing 2013.
- [22] Grądziel S., Majewski K.: *Simulation of heat transfer in combustion chamber waterwall tubes of supercritical steam boilers*. Chem. Process Eng. **3**(2016), 2, 199–213.
- [23] Grądziel S.: *Selected Issues of Power Boiler Operation*. Wydaw. PK, Kraków 2023 (in Polish)
- [24] Zima W., Nowak-Ocłoń M.: *A new 1D/2D model of the conjugate heat transfer in waterwall tubes of the supercritical steam boiler combustion chamber*. Heat Transf. Eng. **39**(2018), 13–14, 1272–1282.
- [25] Majdak M., Grądziel S.: *Analysis of thermal flow in waterwall tubes of the combustion chamber depending on the fluid parameters*. Therm. Sci. **23**(2019), 1333–1344.
- [26] Majdak M.: *Thermal flow and strength analysis of combustion chamber waterwall tubes operation*. PhD thesis, Cracow University of Technology, Kraków 2021 (in Polish).
- [27] Wilo SE: *Wilo Stratos GIGA 40/1-45/3,8*. <https://wilo.com/id/en/Products-and-expertise/en/products-expertise/wilo-stratos-giga/stratos-giga-40-1-45-3-8> (accessed 20 Oct. 2023).
- [28] GOTRONIK PPHU: *Power regulator parameters (BTE-435)*. <https://www.gotronik.pl/modul-regulatora-mocy-10000w-p-4278.html> (accessed 20 Oct. 2023).
- [29] ENKO-POMIAR Sp. z o.o.: *Electromagnetic flow meters*. <https://www.enko-pomiar.pl/52,81,0> (accessed 20 Oct. 2023).
- [30] ALF-SENSOR Sp. J.: *Thermocouples*. <https://alf-sensor.com/catalogue-of-our-products/thermocouples.html> (accessed 20 Oct. 2023).
- [31] Ahlborn ALMEMO MA 5690-2 Manual. <https://www.ahlborn.com/download/anleitung/eng/56902e.pdf> (accessed 20 Oct. 2023).
- [32] AMR Win Control software. <https://www.ahlborn.com/download/pdfs/kap05/eng/WinControle.pdf> (accessed 20 Oct. 2023).